

REPORT DOCUMENTATION PAGE			Form Approved OMB No. 0704-0188	
<small>Public reporting burden for this collection of information is estimated to average 1 hour per response, including the time for reviewing instructions, searching existing data sources, gathering and maintaining the data needed, and completing and reviewing the collection of information. Send comments regarding this burden estimate or any other aspect of this collection of information, including suggestions for reducing this burden, to Washington Headquarters Services, Directorate for Information Operations and Reports, 1215 Jefferson Davis Highway, Suite 1204, Arlington, VA 22202-4302, and to the Office of Management and Budget, Paperwork Reduction Project (0704-0188), Washington, DC 20503.</small>				
1. AGENCY USE ONLY (Leave blank)	2. REPORT DATE July 1996	3. REPORT TYPE AND DATES COVERED Technical, 9/93-6/97 <i>Final</i>		
4. TITLE AND SUBTITLE Fundamental Studies in Crack Initiation		5. FUNDING NUMBERS <i>F49620 -</i> 92-J-0493		
6. AUTHOR(S) John Botsis		AFOSR-TR-96 <i>0368</i>		
7. PERFORMING ORGANIZATION NAME(S) AND ADDRESS(ES) Dept. of Civil and Materials Engineering University of Illinois at Chicago 842 West Taylor Street Chicago, IL 60607		10. SPONSORING/MONITORING AGENCY REPORT NUMBER <i>F49620 -</i> <i>92-J-0493</i>		
9. SPONSORING/MONITORING AGENCY NAME(S) AND ADDRESS(ES) AFOSR/NA 110 Duncan Avenue, Suite B115 Bolling AFB DC 20332-0001		<i>NA</i>		
11. SUPPLEMENTARY NOTES				
12a. DISTRIBUTION/AVAILABILITY STATEMENT Approved for public release, Unclassified distribution unlimited		12b. DISTRIBUTION CODE DISTRIBUTION STATEMENT A Approved for public release Distribution Unlimited		
13. ABSTRACT (Maximum 200 words) Damage evolution before crack initiation in an amorphous polymer show that damage consists of a core of highly dense crazing and peripheral less dense zone of crazing. Analysis of the kinematics of damage at different times involves comparisons of the inertia moments of damage distributions. The results indicate that damage evolution can be approximated by a linear transformation of the space variables. The crack initiates within a core zone immediately ahead of the notch. The experimental results suggest that damage density within the core is independent of the loading conditions considered herein. An energy release rate is evaluated with the use of a semi-empirical method. Correlation of the elementary movements of the damage zone with the energy release rate shows that damage growth decreases monotonically. Assuming that damage evolution is a stress - temperature driven process, it is shown that a first order reaction equation describes reasonably well damage growth within the core zone. An activation energy for defect nucleation is found twice the enthalpy of activation for secondary chain motions below glass transition. This result indicates that chain motions and chain scission are possible process leading to crack initiation.				
14. SUBJECT TERMS crack initiation, fatigue, damage, kinematics		15. NUMBER OF PAGES <i>46</i>		
		16. PRICE CODE		
17. SECURITY CLASSIFICATION OF REPORT Unclassified	18. SECURITY CLASSIFICATION OF THIS PAGE Unclassified	19. SECURITY CLASSIFICATION OF ABSTRACT Unclassified	20. LIMITATION OF ABSTRACT <i>✓</i>	

NSN 7540-01-280-5500

Standard Form 298 (Rev. 2-89)
Prescribed by ANSI Std. Z39-18
298-102

19960726 054

DTIC QUALITY INSPECTED 1

Fundamental Studies in Crack Initiation

ABSTRACT

Mechanistic investigations of damage evolution before crack initiation in an amorphous polymer show that damage consists of a core of highly dense crazing and a peripheral less dense zone of crazing. Damage characterization is carried out at consecutive configurations of the damage zone. Analysis of the kinematics of damage at different times involves comparisons of the inertia moments of damage distributions. The results indicate that damage evolution between consecutive configurations can be approximated by a linear transformation of the space variables. Thus, the process of damage growth can be described by translation and deformation of the damage zone. The growth rates of the damage zone movements decrease until crack initiation. In all cases, the average densities exhibit a damping type behavior with the number of cycles. The crack initiates within a core zone immediately ahead of the stress concentrator. The experimental results suggest that damage density within the core zone is independent of the loading conditions considered herein. This value is approximately equal to the damage density around the crack tip during slow crack propagation. The crack length at initiation is found to increase exponentially with the stress level. A simple decaying exponential relationship relates the crack initiation times and the applied stress level. This result is consistent with the fracture models based on absolute reaction theories.

An energy release rate due to damage growth before crack initiation is evaluated with the use of a semi-empirical method for energy calculations and experimental measurements. Correlation of the elementary movements of the damage zone with the energy release rate shows that the rate of damage growth decreases monotonically. This is consistent with the growth behavior of an average damage density within the zone. The experimental data have shown that crack initiation occurred when damage density within a core zone ahead of the notch tip reached a critical level, independent of loading conditions. Assuming that damage evolution is a stress - temperature driven process, it is shown that a first order reaction equation describes reasonably well damage growth within the core zone. The rate constants are evaluated by invoking principles of kinetic theories of fracture and experimental results on crack initiation times. An activation energy for defect nucleation is found half the energy for thermal destruction and twice the enthalpy of activation for secondary chain motions below glass transition temperature. This result indicates that chain motions and chain scission are possible rate determining process leading to crack initiation. This is consistent with the observation that dense crazing precedes crack initiation.

SIGNIFICANT FINDINGS

1. A damage zone accompanied the process of crack initiation. Within the zone two patterns of damage were distinguished: a core of highly dense damage and a peripheral less dense crazes around the core zone. Crack initiation occurred within the core zone.
2. Damage evolution before crack initiation evolved in a self - similar manner. That is, a linear transformation related the points of equal damage at consecutive configurations of damage.
3. While the growth behavior of the damage zone center depended upon the loading history, the average rates of the damage zone expansion and distortion decreased until crack initiation. Moreover, the dependency of an average damage density with the cycle number exhibited a damping behavior.
4. Damage density within the core of damage was found independent of the loading conditions, however, the pattern of the peripheral crazes was dependent upon the loading conditions. The large difference in crack initiation times was attributed to the role of time dependent processes within the damage zone and the interaction between the crazes.
5. The crack length at initiation was found to increase exponentially with the applied stress.
6. The time to crack initiation was related to the stress level with an exponentially decaying relationship. The results agree with fracture models based on reaction theories.
7. Using a number of assumptions regarding craze openings and a semi - empirical method, an energy release rate corresponding to damage growth before crack initiation was evaluated. Correlation of the energy release rate with the elementary movements of the damage zone showed that the overall behavior of damage growth before crack initiation decreased with energy release rate. This trend is consistent with the growth behavior of an average damage density before crack initiation.
8. The data showed that damage evolution within the core zone can be approximated by a first order kinetic equation.
9. An activation energy for defect nucleation was found half the activation energy for thermal destruction and about twice the enthalpy of activation for secondary polymer chain movements. This result suggested that secondary chain motion and scission are the rate determining processes leading to crack initiation.

The results of the present studies and those reported in [17, 18] indicate certain similarities between the characteristics of damage before crack initiation and during slow crack growth. These are, (a) damage evolution can be described by a linear transformation, (b) the densities of damage within a core zone at crack initiation and during slow crack growth are of the same level.

TABLE OF CONTENTS

ABSTRACT.....	i
SIGNIFICANT FINDINGS.....	ii
TABLE OF CONTENTS.....	iii
LIST OF TABLES.....	iv
LIST OF FIGURES.....	v
1. INTRODUCTION.....	1
2. EXPERIMENTAL PROCEDURES.....	3
MATERIALS AND SPECIMENS.....	3
EXPERIMENTAL METHODS.....	3
3. EXPERIMENTAL RESULTS AND DISCUSSION.....	5
4. ANALYSIS.....	27
ENERGY EVALUATIONS.....	27
KINETIC CHARACTERISTICS OF DAMAGE IN THE CORE ZONE.....	33
REFERENCES.....	44

LIST OF TABLES

Table I:	Loading Conditions for Crack Initiation Times and Damage Evolution Studies.....	12
Table II:	Inertia Moments for two Configurations of Damage before Crack Initiation.....	12
Table III:	Moment Ratio of Damage Distribution at Consecutive Configurations before Crack Initiation.....	13
Table IV:	Growth Rates of the Gravity Center, Isotropic Expansion and Distortion for three Loading Conditions.....	13
Table V:	Cycle number, Characteristic Size and Energy Release Rates, A. due to Damage Growth for two Loading Conditions.....	38

LIST OF FIGURES

Fig. 1	Schematic of a mesh of rectangles used in damage measurements.....	14
Fig. 2	Series of optical micrographs showing damage growth before crack initiation.....	15
Fig. 3	Contours of equal damage density ρ [mm^2/mm^3], for two specimens fatigued under the same conditions and equal times (Conditions C2).....	16
Fig. 4	Contours of equal damage density ρ [mm^2/mm^3], at four consecutive configurations before crack initiation (Conditions C1).....	17
Fig. 5	Contours of equal damage density ρ [mm^2/mm^3], at three consecutive configurations before crack initiation (Conditions C2).....	18
Fig. 6	Contours of equal damage density ρ [mm^2/mm^3], at three consecutive configurations before crack initiation (Conditions C3).....	19
Fig. 7	Evolution of the gravity center of the damage zone.....	20
Fig. 8	Normalized average density before crack initiation plotted against normalized cycle number.....	21
Fig. 9	Optical micrographs showing damage distribution at crack initiation (Conditions C1).....	22
Fig. 10	Optical micrographs showing damage distribution at crack initiation (Conditions C3).....	23
Fig. 11	Typical morphology of the fracture surface at crack initiation. Arrows point at the crack front (crack grows from top to bottom).....	24
Fig. 12	Crack length at crack initiation for various levels of stress amplitude.....	25
Fig. 13	The time to crack initiation plotted against stress amplitude.....	26
Fig. 14	Schematic of a damage zone around a V- notch.....	39
Fig. 15	(a) Illustration of a displacement response at point x , due to a discontinuity at ξ given by expression (5), (b) Schematic showing the approximation of discontinuities within a rectangle (see text for details).....	40
Fig. 16	Growth rates of the characteristic size, isotropic expansion and distortion of the damage zone vs. energy release rate (Conditions C1).....	41
Fig. 17	Growth rates of the characteristic size, isotropic expansion and distortion of the damage zone vs. energy release rate (Conditions C2).....	42
Fig. 18	Evolution of normalized damage density in the core vs. time for three loading conditions, a (C1), b (C2), and c (C3).....	43

1. INTRODUCTION

Prediction of life time of a structural component subjected to fatigue or creep loads assumes a position of prominence in engineering design. It becomes even more important when considering the continuous increase in complexity of engineering structures and the large costs resulting from premature failures. Thus, characterization of the mechanisms leading to crack initiation and growth is an issue of central importance to engineers and material scientists.

Contemporary approaches to life time prediction consider a fracture process in three phases: crack initiation, slow crack growth, and fast fracture. The latter phase is very short in duration and thus, the time of crack initiation and that of slow crack growth account for the useful time of a structure.

Significant efforts have been devoted to studying slow crack propagation in various materials. This is demonstrated by the vast amount of experimental data and several models that have been proposed to describe crack growth with the stress intensity factor K_I , or energy release rate J_I [1, 2]. These analyses play an important role in life time prediction. However, experimental and theoretical studies of crack initiation have received limited attention in the literature. Moreover, fracture mechanics approaches to fatigue do not consider crack initiation [1]. Instead, the concept of crack growth threshold is employed [3, 4]. Values of fatigue threshold indicate the cyclic stress intensity factor ΔK_{th} , below which long cracks remain dormant. The corresponding ΔK_{th} is taken as a material parameter. Although the study of fatigue thresholds and near threshold behavior has highlighted the effects of load history in influencing crack growth, and has provided insight into the different mechanisms of crack closure, the threshold idea has met with limited success in engineering design. This stems from the fact that the use of a fatigue threshold represents a conservative design criterion and from questions regarding ΔK_{th} as a material parameter [5-7].

Mechanistic investigations in various materials have shown that fatigue crack initiation and growth are preceded by various forms of damage that nucleate at heterogeneities within the material. In metals initiation is related to intense slip processes, extrusions-intrusions and persistent slip bands [8, 9]. Microcracks nucleated at inclusions or second phase particles in the case of smooth specimens have also been reported by several researchers. Observations of the same process in both notched and smooth specimens of polymers have emphasized the role of crazing in amorphous and semi - crystalline polymers [10-13]. Damage nucleation and

growth, whether in the form of microcracks, voids, homogeneous transformations, crazes, etc., are processes that absorb energy, energy that otherwise would be available to drive the crack. Therefore the nature and extent of damage determine the time to crack growth and toughness of the material. Under these circumstances, use of fracture mechanics parameters may not be always justified. That is, when the restrictions of 'K-dominance' or ' J_1 -dominance' are not met, K_1 and J_1 fail to correlate with the fracture process. Examples are large scale plasticity, microcrack interaction, the behavior of small cracks, etc.

Recognizing the importance of damage on crack initiation and growth, several analytical approaches have been developed to account for its effects on stress intensity factor and energy release rates (for a recent review see [14] and references therein). It is difficult, however, to assess the contributions of crack damage interactions, describe the local kinetics, and the effects of the microstructure when a large number of microdefects is present. These powerful mechanisms are the main obstacles in modeling fracture in a large class of modern engineering materials.

One way to treat fracture phenomena where dense damage accompanies crack initiation and growth is to use the ideas of self - similarity. Drawing on the success of statistical self - similarity of vortex cascade in understanding turbulence, it is proposed that the same principles can be applied to damage and fracture of engineering materials [15,16]. Indeed, experimental observations in a number of materials have shown that damage growth displays certain invariant characteristics. For example, the evolution of a normalized pore size distribution in polycrystalline steel under creep follows a pattern that is independent of time and strain level [15]. Furthermore, it has been shown that damage growth within a process zone during fatigue fracture can be described by a self - similar transformation of the space variables [17]. Modeling of such fracture processes has been made by introducing additional kinematic parameters on the basis of self - similarity [16].

Formulations of constitutive equations for damage growth and criteria for crack initiation are well recognized by now to be important problems in fracture research. Although, important progress has been made in this direction, a number of questions still remain to be properly addressed and resolved for a better understanding of fracture. In this two Part series of papers, inquiries into the characteristics of damage evolution before crack initiation and criteria for crack initiation are addressed. In Part I, experimental studies on damage evolution are reported using amorphous polystyrene as a model material. To facilitate experimental observations, the site of crack initiation is located in space by inducing a 60° -V notch onto the mid-span of the specimen

edge. Hence, efforts are concentrated on characterizing damage dissemination, the associated kinematic parameters, and the time to crack initiation. In Part II, the energy release rate due to damage growth is evaluated using of a semi - empirical method and experimental measurements. On the basis of the experimental results damage growth in front of the notch tip is modeled with a first order reaction equation.

2. EXPERIMENTAL PROCEDURES

MATERIAL AND SPECIMENS

Commercially available amorphous polystyrene (PS) from Transilwrap, Chicago, IL, was employed in the studies of crack initiation. The material was received in the form of sheets with dimensions of 200x250 mm. Strips of 150x22x0.20 mm were cut from these sheets with a razor blade and sandwiched between two pieces of acrylic with dimensions 150x21x6.5 mm. The specimens were squared up to 150x20x0.20 mm with the use of a fly cutter on a milling machine. The speeds of the fly cutter and the longitudinal power feed of the working table that supports the specimens were 11 rotation·sec⁻¹. and 0.23 mm·sec⁻¹, respectively. First, sections of about 0.25 mm thick were cut off the block of specimens until the edges of the specimens were on the same plane. The final few cuts were in the order of 0.01 mm so that the induced damage was minimized. The block was then flipped over and the same procedure was repeated until the desired width was achieved. The machined edges were metallographically polished to a 0.5μm finish to prevent formation of edge crazes. A double angle cutter of 60° was used to notch the specimens prior to their removal from the block. Subsequently the specimens were removed from the block and washed carefully with distilled water. Note that this procedure of specimen preparation ensures identical notch tip geometries. Finally, the specimens were annealed in a temperature of 10°C degrees lower than T_g (glass transition temperature) for 48 hours and then allowed to slowly cool down to room temperature. Annealing was aimed at relieving any residual stresses and healing any damage formed during the cutting procedures.

EXPERIMENTAL METHODS

Tension - tension fatigue experiments were conducted on an Instron Testing System in laboratory environment at ambient temperature. All experiments were performed under load controlled mode with sinusoidal wave form. The evolution of damage around the notch tip was observed by means of a traveling optical microscope attached to the Instron Testing System. The fracture process was recorded using a motor driven camera that was attached to the microscope. Craze distribution was

evaluated from optical micrographs of sectioned specimens (approximately 10-20 μ m thick) which were prepared by standard metallographic and polishing procedures. Damage density distributions were obtained by covering the micrographs of the polished sections with a mesh of rectangles. The size of a typical mesh depended upon the extent of damage around the notch tip and was about $N_1 \times N_2 \approx 10 \times 15$ (Figure 1). In all cases the dimensions of the rectangles were approximately 12 \times 12 μ m. In each rectangle, the number of crazes was counted. Craze density was evaluated as number per unit area p [#/ mm^2] or as $\rho = \frac{nbt}{abt}$ [mm^2/mm^3]. ρ represents the amount of area of craze mid planes per unit volume, n is the number of intersections of crazes with the vertical test line at the respective rectangle, a and b were the height and width of a rectangle, respectively, and t is the specimen thickness.

The most direct way to experimentally measure damage growth rates are by examination of sectioned samples that have been exposed to a well controlled loading history. In this way damage growth is "frozen in" at different degrees of development. Thus, to obtain damage distribution and growth rates before initiation, the experiments designed for damage evolution studies were interrupted at appropriate time intervals. Subsequently, the specimens were polished and the number of crazes in each rectangle was evaluated.

The approach of characterizing damage described in the preceding paragraphs implies that, at a given time, damage distribution around the stress concentrator is reproducible for a certain set of loading conditions and specimen geometry. Damage accumulation, however, is a stochastic process. Accordingly, damage distribution should result from averages of a sufficiently large number of distributions observed on identical specimens. However, such an effort is experimentally difficult to carry out. Commercially available PS is a relatively 'ductile' material. This results in a large extent of crazing during crack initiation and slow crack growth [17,18]. Thus, damage within a zone in this material is amenable to a statistical treatment. To examine the reproducibility of damage distribution, two experiments were performed under the same loading conditions and specimen geometry.

The time to crack initiation was examined under the loading histories shown in Table I. Crack initiation was considered when a crack, however small, would appear at the notch tip. This event was observed with the use of a Nikon optical microscope under a magnification of x200. It has been shown that crack initiation time in PS under fatigue loads exhibits a variability of about 10% [19]. This scatter was considered small and thus, efforts were concentrated at investigating damage growth before

initiation under three loading conditions, which are referred to as C1, C2, and C3. Four experiments were conducted under C1 and three under each of C2 and C3 conditions. The loads and frequency for these three sets of experiments are shown in Table I.

Due to difficulties associated with measuring an accurate crack size at initiation using an optical technique, the tests were interrupted shortly after crack initiation. Subsequently, the specimens were pulled to fracture. A crack size at initiation was assessed by examination of the fracture surfaces and its dependence on the stress level was evaluated by performing fatigue tests under different loads.

3. EXPERIMENTAL RESULTS AND DISCUSSION

Upon application of the load, a core zone of crazes appeared at the notch tip. While this zone increased in size, few arched crazes nucleated and propagated around the core zone. As time progressed, the crazes grew longer as well as new crazes appeared in and around the vicinity of the core. A series of optical micrographs taken during a typical experiment is shown in Figure 2. Crack initiation was defined at the instance when a crack appeared at the notch tip.

One way to investigate damage evolution is to compare the contours of equal damage density at consecutive configurations. Such pointwise comparison, however, may not be appropriate because of local fluctuations in damage density. Indeed, the contours of equal damage level at each configuration obtained from different specimens exhibit noticeable fluctuation on the scale of several micrometers (Figures 3 to 7). Therefore integral parameters, such as the moments of damage distribution, were used here to evaluate the properties of damage evolution before crack initiation.

Characterization of any distribution with the use of moments should involve comparison of a sufficiently large number of moments. However, relatively high order moments may not be appropriate to compare because the experimental error built into the measurement makes them relatively inaccurate. In the present analysis, the distributions of damage were characterized by the total number of crazes within the zone l_0 , the second l_{2x} , l_{2y} and fourth l_{4x} , l_{4y} , and l_{2x2y} central moments. These quantities were evaluated from the following expressions,

$$l_0 = \sum_{i=1}^{N_1} \sum_{j=1}^{N_2} p_{ij}, \quad l_{m \times n} = \sum_{i=1}^{N_1} \sum_{j=1}^{N_2} [x_{ij} - x_c]^m [y_{ij} - y_c]^n p_{ij} \Delta y_j \Delta x_i$$

Here $i = 1, \dots, N_1$ and $j = 1, \dots, N_2$ refer to the size of the mesh (see Figure 1) and m, n stand for the order of the moments and take values of, 0, 2, or 4. x_c and y_c are the coordinates of the damage zone center with reference to the notch tip and given by,

$$x_c = \frac{\sum_{i=1}^{N_1} \sum_{j=1}^{N_2} x_{ij} p_{ij} \Delta y_j \Delta x_i}{\sum_{i=1}^{N_1} \sum_{j=1}^{N_2} p_{ij} \Delta y_j \Delta x_i}, \quad y_c = 0$$

y_c is zero due to symmetry of the damage zone around the y axis (Figure 3).

The contours of equal damage density ρ , pertaining to two specimens fatigued under conditions C2 (Table I) and up to the instance of crack initiation are displayed in Figure 3. Note that, the contours of damage density have been symmetrized with respect to the bisector of the V-notch because small variations in density were observed at some points located at equal distances from the X axis. These differences were attributed to local fluctuation in damage density. Thus, the density at these locations was substituted with the arithmetic mean of the respective density values. For the sake of visual clarity, the level of experimental error is not shown in Figures 3 to 6. The error in the measurements of craze density far from the notch tip was about 10%. For the measurements near the notch tip, the error was about 15 - 20%. The larger value of error was because the high craze density in the close vicinity of the notch tip limits optical microscopy which makes accurate measurements difficult. From these data moments of the distribution with respect to the center of the zone as well as the notch tip were evaluated (Table II). A comparison of the moments shown in Table II shows that the largest difference is ~10% and occurred between the I_{4x} moments with reference to the notch tip. The rest of the differences were always less than 10%. These data and the reproducibility of damage distribution within a process zone in the same material [17] were taken as sufficient indications that damage distributions during crack initiation were reproducible.

Measurements of damage density within the zones yielded the contours of equal density, ρ , that are shown in Figures 4, 5, and 6, for conditions C1, C2 and C3, respectively. From the experimental data presented in these Figures the center of the damage zone, x_c , can be calculated at each configuration. The data in Figure 7 indicate that the center of gravity of the damage zone increased monotonically with the number of cycles. To investigate the type of transformation the damage density is undergoing during its evolution, the following characteristic scales along the X and Y axes are defined,

$$\frac{I_{2x}}{I_0} = \sigma_x^2, \quad \frac{I_{2y}}{I_0} = \sigma_y^2$$

Since I_{2x} , I_{2y} are the second moments of the damage zone and I_0 is the zeroth moment (which expresses the total amount of crazes within the damage zone) σ_x and σ_y can be looked upon as the measurements of damage spread in the X and Y axes, respectively. Accordingly, for the purpose of comparing damage distributions within the damage zone the following ratios were defined between i_{th} and j_{th} configurations ($i = 1, 2, 3$ and $j = i+1$),

$$\frac{\sigma_x^{(i)}}{\sigma_x^{(j)}} = \lambda_{ji}, \quad \frac{\sigma_y^{(i)}}{\sigma_y^{(j)}} = \mu_{ji}, \quad \frac{I_{4x}^{(i)}/I_0^{(i)}}{I_{4x}^{(j)}/I_0^{(j)}} = \Lambda_{ji}^4, \quad \frac{I_{4y}^{(i)}/I_0^{(i)}}{I_{4y}^{(j)}/I_0^{(j)}} = M_{ji}^4, \quad \frac{I_{2x2y}^{(i)}/I_0^{(i)}}{I_{2x2y}^{(j)}/I_0^{(j)}} = H_{ji}^4$$

The type of transformation of damage distribution between consecutive configurations was examined by comparing the following quantities: $(\lambda_{ji}, \Lambda_{ji})$, (μ_{ji}, M_{ji}) , and $(\lambda_{ji}\mu_{ji}, H_{ji}^2)$. The above defined ratios for conditions C1, C2, and C3 are shown in Table III. The data in Table III indicate a relatively large difference in the ratios between the first and second configurations for conditions C1. This may be because the system needs some time for damage to be developed so that statistical measurements are meaningful. However, differences between the rest of the ratios were small.

The constancy of the ratios λ_{ji} , μ_{ji} between configurations shown in Table III implied that the evolution of damage can be approximated by a linear transformation of the space variables. To obtain the kinematic parameters, the velocity $V_m(\mathbf{x})$ of a point within the zone is expressed by the first two terms of Taylor series around the center of the damage zone,

$$V_m(\mathbf{x}) \approx V_m(0) + V_{m,n}(\mathbf{x})x_n \quad (3.1)$$

Here, the first term represents the rigid translation of the damage zone and the second term represents the rotation (anti-symmetric part of $V_{m,n}$) and the deformation (symmetric part of $V_{m,n}$) which in turn can be decomposed into isotropic expansion and homogeneous distortion of the damage zone. In this section the velocity $V_m(\mathbf{x})$ is expressed in terms of the transformation coefficients λ_{ji} and μ_{ji} . Subsequently the rates of expansion and distortion are evaluated.

The transformation matrix of points with equal damage density between configuration i and j is,

$$D = \begin{bmatrix} \lambda_{ji} & 0 \\ 0 & \mu_{ji} \end{bmatrix} \quad (3.2)$$

which can be rewritten as,

$$D = \begin{bmatrix} 1 + \Delta\lambda_{ji} & 0 \\ 0 & 1 + \Delta\mu_{ji} \end{bmatrix} = I + \Delta D \quad (3.3)$$

where I is the identity matrix and,

$$\Delta D = \begin{bmatrix} \Delta\lambda_{ji} & 0 \\ 0 & \Delta\mu_{ji} \end{bmatrix} \quad (3.4)$$

Thus, the displacement field within the damage zone can be expressed as,

$$\begin{bmatrix} x + \Delta x \\ y + \Delta y \end{bmatrix} = \begin{bmatrix} 1 + \Delta\lambda_{ji} & 0 \\ 0 & 1 + \Delta\mu_{ji} \end{bmatrix} \begin{bmatrix} x \\ y \end{bmatrix} + \begin{bmatrix} \Delta x_c \\ 0 \end{bmatrix} \quad (3.5)$$

where, Δx_c , represents the growth of the center along the x axis. Equation (3.5) can be rewritten as,

$$\begin{bmatrix} \Delta x \\ \Delta y \end{bmatrix} = \begin{bmatrix} \Delta\lambda_{ji} & 0 \\ 0 & \Delta\mu_{ji} \end{bmatrix} \begin{bmatrix} x \\ y \end{bmatrix} + \begin{bmatrix} \Delta x_c \\ 0 \end{bmatrix} \quad (3.6)$$

Dividing both sides by the increment of the cycle number ΔN , and setting $\frac{\Delta x}{\Delta N} \rightarrow V_1$,

$\frac{\Delta y}{\Delta N} \rightarrow V_2$, $\frac{\Delta\lambda_{ji}}{\Delta N} \rightarrow \dot{\lambda}_{ji}$, $\frac{\Delta\mu_{ji}}{\Delta N} \rightarrow \dot{\mu}_{ji}$, $\frac{\Delta x_c}{\Delta N} \rightarrow \dot{x}_c$ it is obtained,

$$\begin{bmatrix} V_1 \\ V_2 \end{bmatrix} = \begin{bmatrix} \dot{\lambda}_{ji} & 0 \\ 0 & \dot{\mu}_{ji} \end{bmatrix} \begin{bmatrix} x \\ y \end{bmatrix} + \begin{bmatrix} \dot{x}_c \\ 0 \end{bmatrix} \quad (3.7)$$

A comparison of Equations (3.1) and (3.7) results in,

$$V_m(\mathbf{x}) = \begin{bmatrix} V_1 \\ V_2 \end{bmatrix}, \quad V_m(0) = \begin{bmatrix} \dot{x}_c \\ 0 \end{bmatrix}, \quad V_{m,n}(\mathbf{x}) = \begin{bmatrix} \dot{\lambda}_{ji} & 0 \\ 0 & \dot{\mu}_{ji} \end{bmatrix} \quad (3.8)$$

Thus, the rates of expansion \dot{e} , and distortion \dot{d} , of the damage zone can be expressed as,

$$\dot{e} = \frac{1}{2}(\dot{\lambda}_{ji} + \dot{\mu}_{ji}), \text{ and } \dot{d} = \frac{1}{2}(\dot{\lambda}_{ji} - \dot{\mu}_{ji}) \quad (3.9)$$

The average values of \dot{e} and \dot{d} as well as the growth of the gravity center of the damage zone for three loading conditions are displayed in Table IV. The data in Table IV show that while the growth behavior of $\Delta X_c/\Delta N$ depended upon the loading history, the average rates of the damage zone deformation, $\Delta e/\Delta N$ and $\Delta d/\Delta N$, decreased until crack initiation.

It is worth pointing out that damage evolution within a process zone on the same material can be described by a linear transformation [17]. These findings and the results of the present studies indicate that a similar transformation relates damage evolution before crack initiation and during slow crack growth.

The evolution of an average damage density $\langle p \rangle = \Sigma/A$, where Σ is the total number of crazes within the zone and A is the area of the zone with normalized cycle number is shown in Figure 8. (Note that because of the large difference in the cycles to crack initiation between the different experimental conditions, C1: 300,000 cycles, C2: 30,000, C3: 4,000, the number of cycles has been normalized with the respective cycle number at initiation in order to clearly see the trend of $\langle p \rangle$). It is interesting to note that all three sets of data can be approximated by an equation of the form (lines in Figure 8),

$$\langle p \rangle = 1 - \exp(-K'N) \quad (3.10)$$

where N is the number of cycles and K' is a load dependent parameter and equal to $K' = 2.5 \times 10^{-5}$ (C1), 8×10^{-5} (C2), and 1.5×10^{-3} cycle⁻¹(C3). Expression (3.10) indicates that the dependency of $\langle p \rangle$ on the cycle number is of a damping character. Similar trends of damage accumulation have been reported on smooth specimens of different polymers under creep loads [20].

The data in Figure 8 show that while the rates of damage accumulation were different, craze densities $\langle p \rangle$, at crack initiation were 40,000, 44,200 and 47,000 mm⁻², respectively. Note that the error between the extreme values of these densities was 16% while the largest difference from the mean was about 10%. Thus one may be led to consider the value of $\langle p \rangle$ as being independent of the loading conditions at crack initiation. This would be realistic if the density within the zone was constant throughout

the zone. However, the results of these studies clearly indicate that damage was not homogeneously distributed (Figures 3 to 6). Thus, an average quantity like $\langle p \rangle$ may not be indicative of the crack initiation event. On the other hand, crack initiation occurred within a core zone ahead of the notch tip. Morphologies of this highly localized damage zone at initiation for conditions C1 and C3 are shown in Figures 9 and 10, respectively. Within the resolution of the experimental measurements, damage density within the core was about $1,300 \text{ mm}^2/\text{mm}^3$ and approximately the same for all loading conditions (Figures 4 to 6). Similar value of damage density has been obtained in the close proximity of the crack tip grown under low frequency fatigue loads [17]. The constancy suggests that a certain level of damage density is required for crack initiation and subsequent crack growth and that this density may be a material parameter. Additional experimental as well as theoretical research is needed to firmly establish this important observation.

The optical micrographs in Figures 9 and 10 bring out an interesting observation. While the density at the notch tip was practically the same, the cycle numbers to crack initiation were drastically different, i. e., 300,000 and 4,000 cycles, respectively. Moreover, damage dissemination around the core zone was quite different (Figures 9 and 10). Thus, one would expect that in the case where large crazes surrounded the core zone would take longer to initiate a crack (Figure 10) due to a greater extent of shielding of the peripheral crazes on the core. However, this was not the case. Therefore, it is assumed that time dependent processes within the damage zone play a more important role than the interaction between the crazes.

It was stated earlier that a small crack was observed at the notch tip. This event was associated with crack initiation. An accurate initial crack size, however, was difficult to detect with the use of standard optical observations during the fatigue tests. To evaluate an initial crack size, the specimens were pulled to fracture shortly after crack initiation and the fracture surfaces were observed under an optical microscope. A typical micrograph of the fracture surface morphology near the notch tip is displayed in Figure 11. Note that two distinct morphologies can be seen in the fracture surface: (i) a relatively rough surface from the notch tip which extends up to an arched front, and (ii) the surface with tearing like features. It is assumed that the first morphology is associated with crack initiation. The second morphology corresponds to the crack growth phase resulting from the simple pulling of the specimen after initiation. The morphology shown in Figure 11 suggested that the crack front was not straight. Instead, crack grows more in the middle than at the edges of the specimen surface. The crack length at initiation l_i , taken as the average of five measurements from the

notch tip to the curved front is shown in Figure 12 as a function of the stress amplitude. These data indicate that the dependence of the crack length on the applied stress is of the form, $\ln l = B_0 + B_1 \sigma$ where B_0 and B_1 are constants.

Crack initiation times τ_i , plotted against the stress amplitude are shown in Figure 13 (note that $N_i = v\tau_i$ where N_i is the number of cycles for crack initiation and v is the test frequency). These data show that τ_i can be approximated by an expression of the form, $\ln \tau_i = D_0 - D_1 \sigma$ where D_0 , and D_1 are parameters. Similar relationships have been obtained for different materials including polymers and metals under constant loads and different temperatures [21,22] and have been explained in terms of stress - temperature activated processes at the molecular level. It may be expected that such a relation would not apply in fatigue loads. However, the frequency of the fatigue experiments was very low. Thus, it may be that the material's response is primarily due to the time under load and less due to cycle reversal. Similar results were obtained under cyclic loads in PANB rocket propellant material [23] and other polymeric solids [24].

TABLE I: Loading Conditions for Crack Initiation Times and Damage Evolution Studies

σ_{\max} (MPa)	σ_{\min} (MPa)	Frequency (sec ⁻¹)	Cycles to Initiation (x10 ³)
C1: 8.00	2.75	0.33	300±10
C2: 10.50	2.75	0.33	30±2.5
C3: 14.30	2.75	0.33	4±0.5
12.00	3.00	0.33	20±2.0
13.00	3.00	0.33	10±1.2

TABLE II: Inertia Moments for two Configurations of Damage before Crack Initiation

Configuration	1	2	1	2
Reference	Notch Tip	Notch Tip	Damage Zone Center	Damage Zone Center
X_c (μm)	55.0	52.0		
Y_c	0.0	0.0		
I_0 (number)	732	680		
I_{2x} (mm ²)	2.8	2.5	0.65	0.63
I_{2y} (mm ²)	0.46	0.42	0.46	0.42
I_{4x} (mm ⁴)	0.20x10 ⁻¹	0.18x10 ⁻¹	0.11x10 ⁻²	0.11x10 ⁻²
I_{4y} (mm ⁴)	0.57x10 ⁻³	0.52x10 ⁻³	0.57x10 ⁻³	0.52x10 ⁻³
I_{2x2y} (mm ⁴)	0.21x10 ⁻²	0.18x10 ⁻²	0.40x10 ⁻³	0.39x10 ⁻³

TABLE III: Moment Ratio of Damage Distribution at Consecutive Configurations before Crack Initiation

Condition C1					
$\lambda_{21}=1.20$	$\Lambda_{21}=1.15$	$\mu_{21}=1.02$	$M_{21}=1.02$	$\lambda_{21} \mu_{21}=1.22$	$H_{21}^2=1.15$
$\lambda_{32}=1.57$	$\Lambda_{32}=1.55$	$\mu_{32}=1.30$	$M_{32}=1.34$	$\lambda_{32} \mu_{32}=2.04$	$H_{23}^2=2.07$
$\lambda_{43}=1.43$	$\Lambda_{43}=1.46$	$\mu_{43}=1.30$	$M_{43}=1.30$	$\lambda_{43} \mu_{43}=1.86$	$H_{43}^2=1.90$
Condition C2					
$\lambda_{21}=1.11$	$\Lambda_{21}=1.10$	$\mu_{21}=1.22$	$M_{21}=1.15$	$\lambda_{21} \mu_{21}=1.35$	$H_{32}^2 = 1.28$
$\lambda_{32}=1.17$	$\Lambda_{32}=1.17$	$\mu_{32}=1.23$	$M_{32}=1.23$	$\lambda_{32} \mu_{32}=1.44$	$H_{32}^2=1.41$
Condition C3					
$\lambda_{21}=1.60$	$\Lambda_{21}=1.58$	$\mu_{21}=1.38$	$M_{21}=1.34$	$\lambda_{21} \mu_{21}=2.21$	$H_{21}^2 = 2.10$
$\lambda_{32}=1.45$	$\Lambda_{32}=1.55$	$\mu_{32}=1.36$	$M_{32}=1.45$	$\lambda_{32} \mu_{32}=1.97$	$H_{32}^2 = 2.25$

TABLE IV: Growth Rates of the Gravity Center, Isotropic Expansion and Distortion for three Loading Conditions

Configuration	$\Delta X_G/\Delta N$ ($\times 10^4$) ($\mu\text{m}/\text{cycle}$)	$\Delta e/\Delta N$ ($\times 10^6$) 1/cycle	$\Delta d/\Delta N$ ($\times 10^6$) 1/cycle
Conditions C1:			
1-2	1.3	13.0	4.4
2-3	1.5	3.0	1.0
3-4	1.6	2.0	0.7
Conditions C2:			
1-2	4.5	20.0	4.5
2-3	11.8	15.0	3.6
Conditions C3:			
1-2	141.5	27.0	48.0
2-3	4.5	1.75	3.0

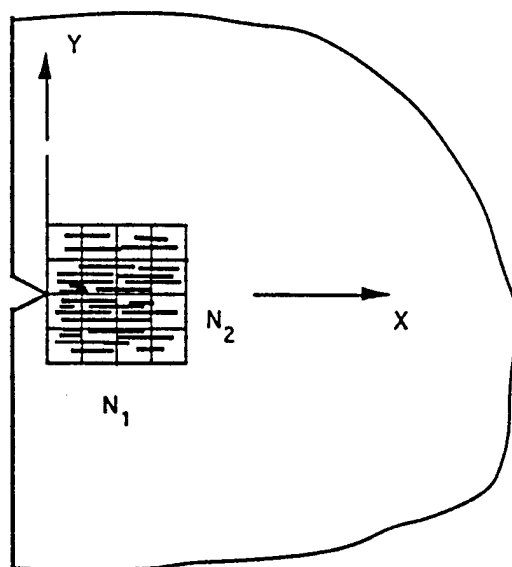
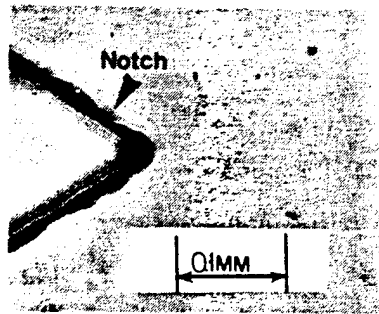


Fig. 1 Schematic of a mesh of rectangles used in damage measurements



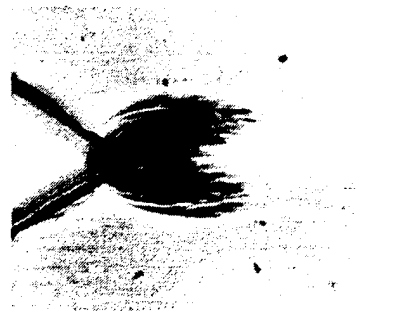
Cycles: 0



Cycles: 130



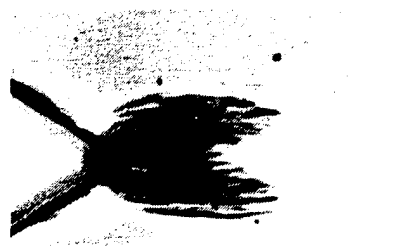
Cycles: 250



Cycles: 23,040



Cycles 38,760



Cycles: 39,430

Fig. 2 Series of optical micrographs showing damage growth before crack initiation

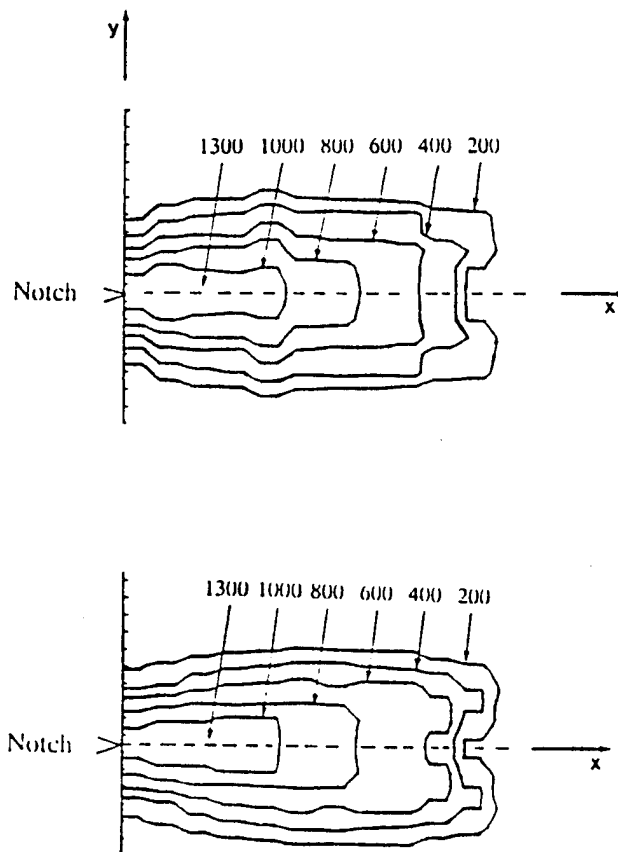


Fig. 3 Contours of equal damage density ρ [mm^2/mm^3], for two specimens fatigued under the same conditions and equal times (Conditions C2)

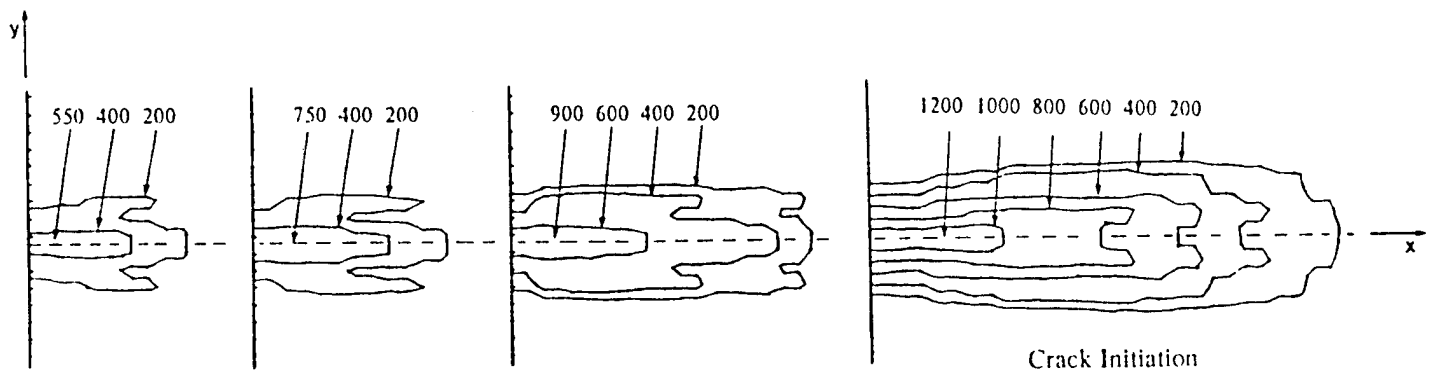


Fig. 4 Contours of equal damage density p [mm^2/mm^3], at four consecutive configurations before crack initiation (Conditions C1)

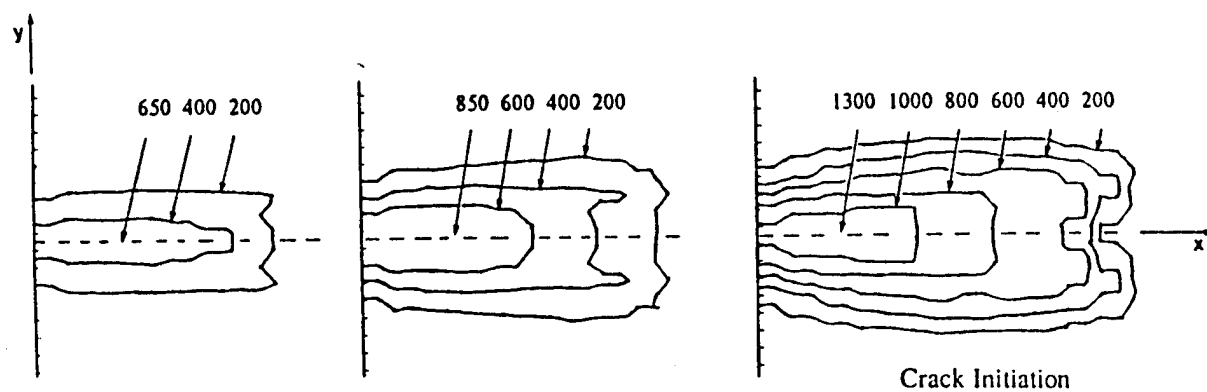


Fig. 5 Contours of equal damage density ρ [mm^2/mm^3], at three consecutive configurations before crack initiation (Conditions C2)

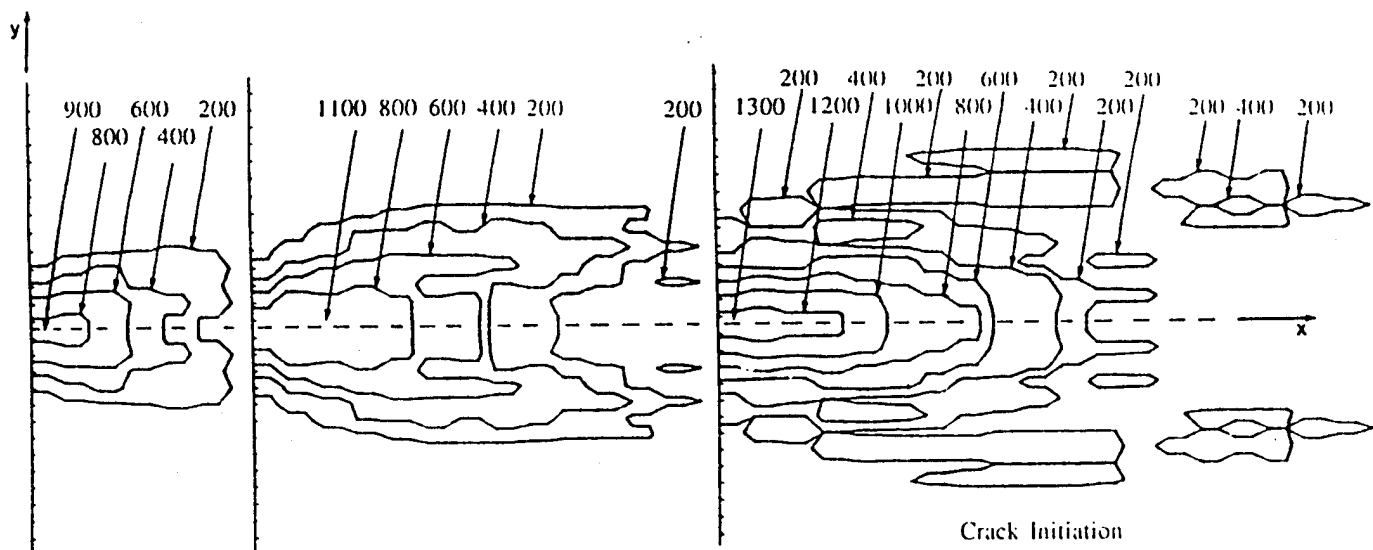


Fig. 6 Contours of equal damage density p [mm^2/mm^3], at three consecutive configurations before crack initiation (Conditions C3)

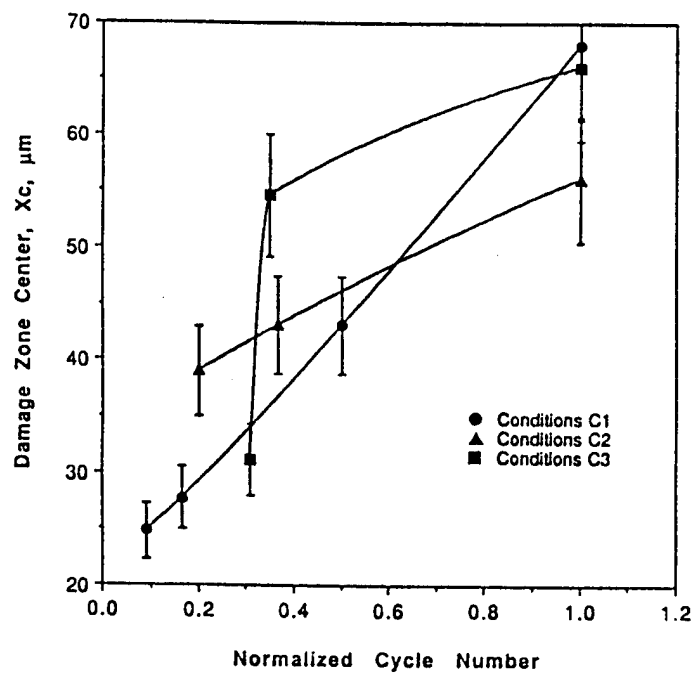


Fig. 7 Evolution of the gravity center of the damage zone

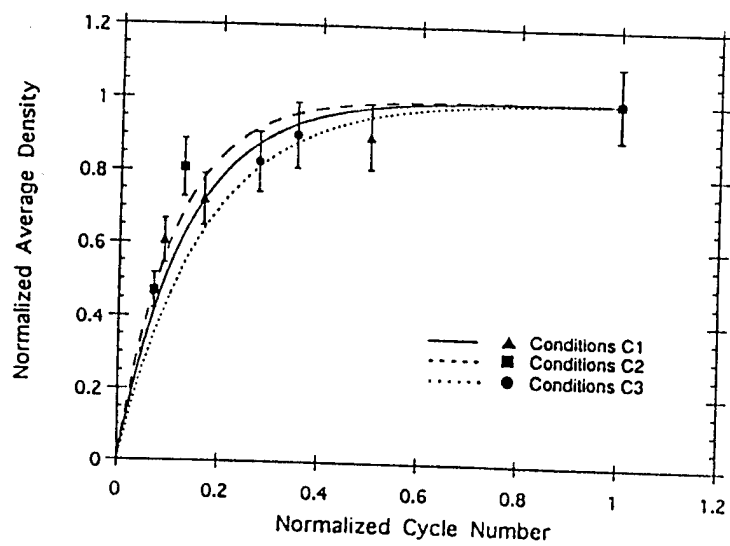


Fig. 8 Normalized average density before crack initiation plotted against normalized cycle number

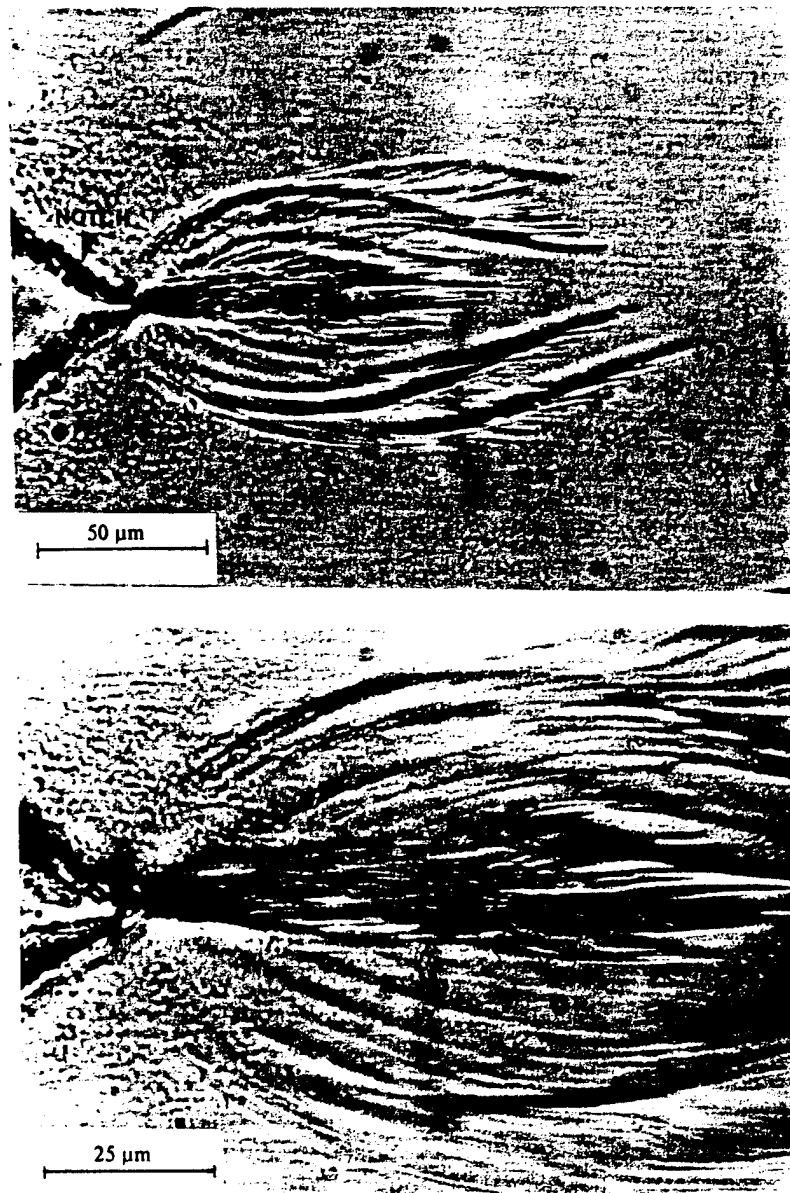


Fig. 9 Optical micrographs showing damage distribution at crack initiation (Conditions C1).

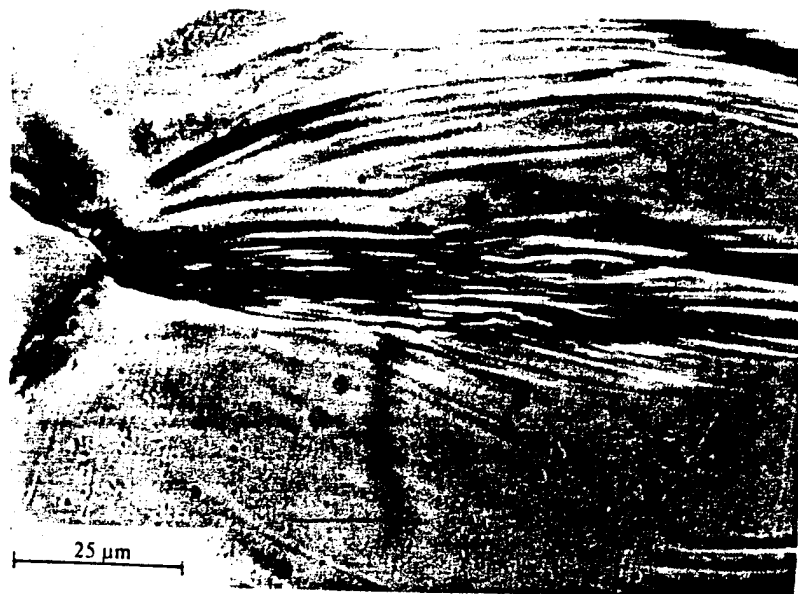
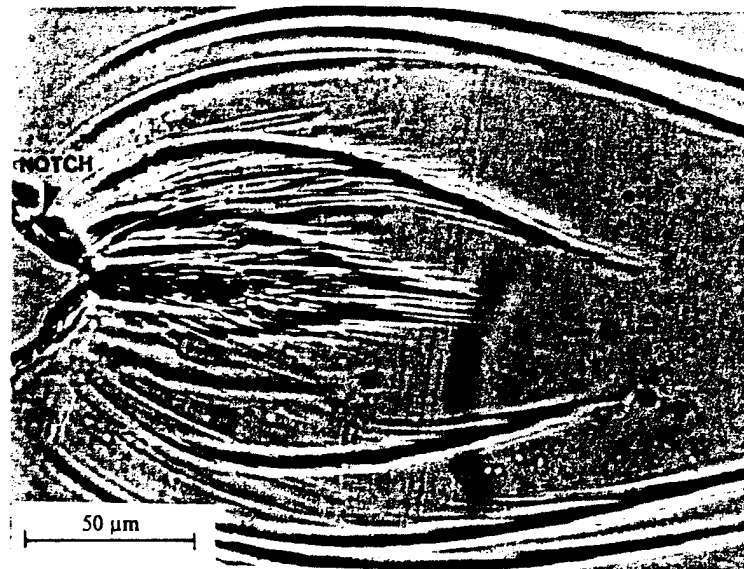


Fig. 10 Optical micrographs showing damage distribution at crack initiation (Conditions C3)

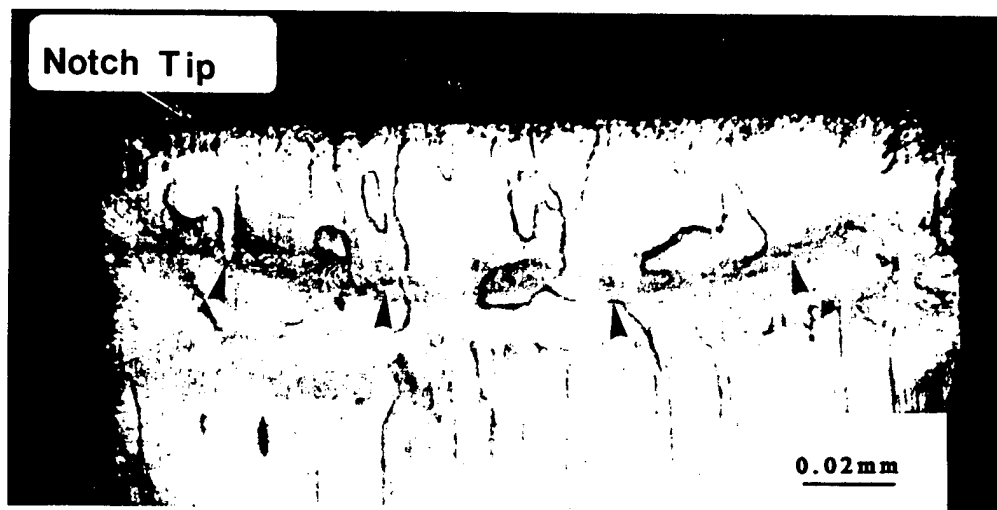


Fig. 11 Typical morphology of the fracture surface at crack initiation. Arrows point at the crack front (crack grows from top to bottom)

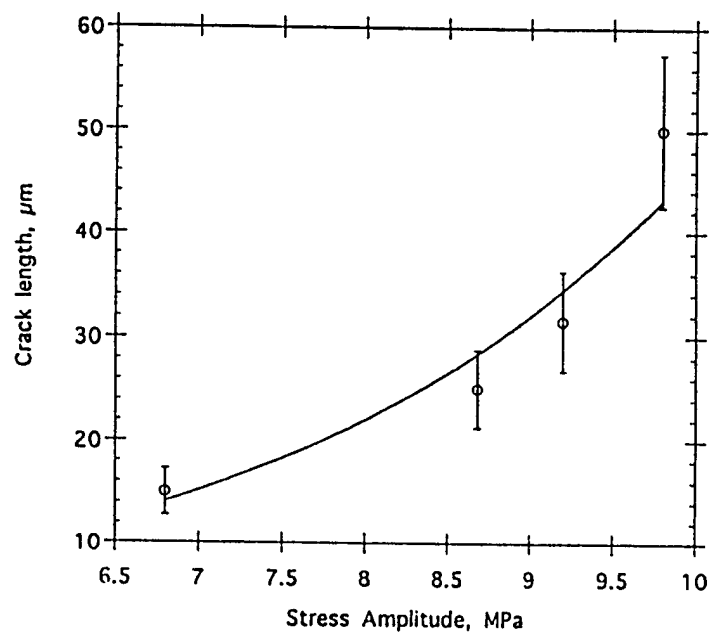


Fig. 12 Crack length at crack initiation for various levels of stress amplitude.

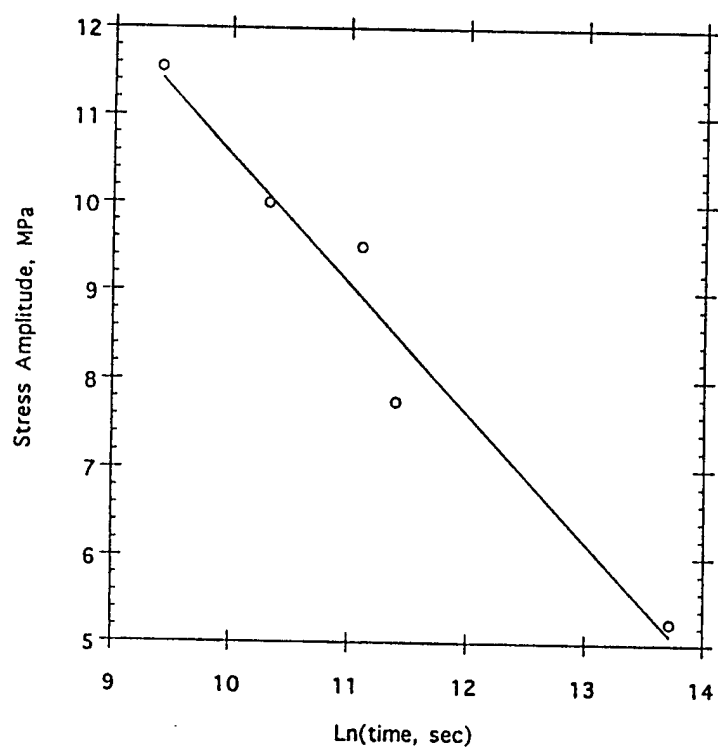


Fig. 13 The time to crack initiation plotted against stress amplitude

4 ANALYSIS

ENERGY EVALUATIONS

The experimental results reported in the last section [25] demonstrated that during the process of crack initiation in amorphous polystyrene (PS) two distinct craze patterns appeared around the stress concentrator; a core zone of dense crazes located in front of the notch tip and peripheral, less dense crazes, surrounding the core. A typical schematic of damage before crack initiation is shown in Figure 14. While the extent of the peripheral crazes depended on the loading history, the density within the core zone at initiation was found, to a good degree of approximation, independent of the loading conditions. Moreover, it was shown that damage evolution before crack initiation can be described by a self - similar transformation. These results allowed to deduce the movements of the damage zone to, translation, isotropic expansion, and homogeneous distortion [25]. Although, these results provided important information in the efforts to characterize the crack initiation process, a further understanding requires calculation of the energy release rates associated with these kinematic parameters. Knowledge of the energy release rates would allow to formulate kinetic equations for damage growth.

Calculation of the stress and strain fields in an elastic body with defects is the first step towards the evaluation of the energy release rates or stress intensity factors. However, such a task is not always easy to accomplish. The complex interaction between the damage elements and the crack makes an analytical solution very difficult to obtain. Therefore, various approximations have been proposed in the literature. In works reported in [26-28], damage is modeled by an effective inclusion. The properties of the inclusion, however, are not easily determined experimentally. In addition, a substitution of an array of defects by a homogeneous medium may not be realistic when defect distribution within a damage zone is heterogeneous. In references [29-33], solutions for the stress and strain fields are based on a detailed description of the defect size, location, and orientation. The mathematical difficulties involved in such a description are enormous and solutions to certain configurations of crack - microcrack systems are possible. In an approach reported in [34], a zone of defects around a crack is characterized by statistical distributions of defect density, size, and orientation. Average parameters are then introduced to model the effects of a damage zone on energy release rates or stress intensity factors. However, when a large number of defects is present, it is difficult to produce experimentally accurate distributions. A semi - empirical analysis has also been proposed to evaluate an energy release rate due to damage growth [35]. It is based on crack or craze openings

and the double layer potential technique. This method was used in the present work as a first approximation to estimate energy changes due to damage using the experimental data and certain assumptions regarding craze openings.

An important aspect of the initiation process is the condition under which crack initiation takes place. Although various mechanisms have been proposed in the literature to explain crack initiation in different materials, quantitative descriptions of initiation have been difficult to formulate. In a physically sound model presented in [36] crack initiation is taken as the instance when the sum of the displacements of the accumulated dipoles before initiation exceeds the theoretical displacement to cause fracture in a perfect crystal. The model derives expressions for the time to crack initiation and the length of the initiated crack and is in good agreement with experimental results. It is not clear, however, if the model would apply to different modes of fatigue damage. Principles of continuum damage mechanics have also been employed for crack initiation. In these models, it is assumed that a macrocrack appears when the elastic stiffness drops to zero, or when a damage parameter reaches a critical value [37, 38]. However, damage parameters employed in continuum damage mechanics may not always be realistic. Models based on irreversible thermodynamics have also been reported, although, they have not been tested experimentally [39, 40]. Constitutive models for nucleation, growth, and coalescence of various submicroscopic failure processes have also been proposed (for a review see [41]). These models are of two types, (a) failure initiation is activated by stress and/or temperature, and (b) failure initiation is due to plastic deformation. In the stress - temperature models, the effects of a tensile stress on the free energy for thermally activated microscopic processes, such as, atomic bond breaking and/or diffusion of vacancies or polymer chain segments are considered. The plastic deformation models are primarily based on heterogeneous slip due to a shear stress. Typical examples are grain boundary sliding, and plastic deformation around inclusions. Thermally activated processes may also play a role in the plastic deformation models. This is when the initially static dislocation or other defects become mobile upon application of stresses and the associated changes in temperature. These models describe well certain aspects of submicroscopic flaw nucleation and have been used in computer simulations with varying degrees of success [41, 42].

In this paper, a semi - empirical method and the experimental results reported in Sec. 3 are used to evaluate an energy release rate associated with damage growth before crack initiation. Subsequently, the rates of the damage zone movements are

correlated with the energy release rate. Next, attention is focused on modeling the evolution of damage within the core zone (Figure 14). Guided by the experimental results [25] and works by various researchers on fracture of polymeric solids [22, 43-51], it is assumed that the particular fracture process reported in [25] is due to submicroscopic flaw nucleation resulting from thermal fluctuations. Thus, the ideas of fracture kinetics are employed to characterize damage evolution at the core zone with a first order kinetic equation.

The experimental results presented in Part I of these investigations indicated that damage evolution before crack initiation can be described by translation and deformation of the damage zone. Thus, the changes in the total potential energy of the system can be expressed as,

$$- \Delta P_t = J_1 \Delta x_c + M \Delta e + N_{ij} \Delta d_{ij}$$

Here, Δx_c , Δe and Δd_{ij} are the increments of the damage zone center, isotropic expansion, and distortion, respectively, and J_1 , M , and N_{ij} are the corresponding energy release rates. To investigate the evolution of the damage zone before crack initiation these energy release rates should be evaluated. Efforts to calculate these energies have been reported in the literature [34]. However, use of these methods requires an accurate description of the craze length, their distribution, and interaction. Such complete characterization is difficult to carry out in systems where a dense damage zone precedes crack initiation. In this work a total energy release rate A , defined as,

$$- \frac{1}{t} \left(\frac{\Delta P_t}{\Delta l_a} \right)_{l_0} = A \quad (4.1)$$

is evaluated using a semi - empirical analysis and experimental measurements. Here l_a is a characteristic size of the damage zone, l_0 is the notch depth and t is the specimen thickness. With respect to the characteristic size, various length parameters of the damage distribution can be used. For simplicity, l_a is taken as the horizontal distance of the outermost damage contour from the notch tip [1]. Such a quantity is easily evaluated from the experiments and due to self - similarity of damage it accounts for the entire size of the damage zone.

The total potential energy P_t of solid with a crack (or a notch) and an array of microdefects is,

$$P_t = P_c + P_d + P_i + P_0 \quad (4.2)$$

The first two terms of the right hand side are the potential energies associated with the main crack and the array of microdefects, respectively, P_i is the potential energy due to interaction of the crack and microdefects, and P_0 the potential energy of the initial state (i. e., without a crack and microdefects). Each term in (4.2) can be defined as the difference between the strain energy of the solid and the work done by the applied load. For a linear elastic solid, the total potential energy can be written as,

$$P_t = -\frac{1}{2}F\Delta_t \quad (4.3)$$

where F is the boundary load which is taken as, $F = \sigma_{\max}A$ (σ_{\max} is the maximum stress of the fatigue cycle, and A is the specimen's cross section) and Δ_t is the total displacement at the points of load application. Since the load is prescribed, the total displacement at the specimen boundaries are evaluated using a semi - empirical method for energy calculations [35]. To carry out this task, the following simplifications and assumptions are employed,

1. Plane stress elastic deformations are assumed throughout the specimen and within the damage zone.
2. Residual stresses are negligible.
3. The principle of superposition applies.
4. The Green's tensor for the displacement at a point \mathbf{x} due to a unit discontinuity at ξ is not available for a semi - infinite plate. Thus, the displacements at the grips of the specimen are obtained by using the Green's tensor for an infinite plate. This is only an approximation since the damage zone is very close to the notch boundaries (Figure 14) and thus, the stress and strain fields are influenced by these boundaries.

To estimate the extent of the error caused by the specimen boundary, the displacements at the grips of the specimen were calculated for the cases when a crack equal to the notch depth is in middle of the specimen and for a specimen with an edged crack of the same length [52]. The displacements at the grips of the single edge cracked specimen were found greater by 8%. Thus, in the present analysis, the displacements calculated using the Green's tensor for an infinite plate were multiplied by 1.08.

The principle of superposition applied to the problem at hand results in the total displacement,

$$\Delta_t = \Delta_{\text{elastic}} + \Delta_{\text{crack}} + \Delta_{\text{crazes}} \quad (4.4)$$

Next, each term in Equation (4.4) should be evaluated. It was argued earlier that during the process of crack initiation, crack growth from the notch does not occur. Moreover, it is assumed that the deformation due to the bulk of the specimen does not change between configurations. Accordingly, the only contribution to the energy release rate A , is that due to damage growth. With reference to Figure 15a, the displacement vector $U_i(\mathbf{x}, \xi)$ at point \mathbf{x} due to a discontinuity opening $b_j(\xi)$ is given by,

$$U_i(\mathbf{x}, \xi) = \int_s b_j(\xi) \Phi_{ij}(\mathbf{x}, \xi) d\xi \quad (4.5)$$

Here $\Phi_{ij}(\mathbf{x}, \xi)$ is the second Green's tensor which stands for the displacement vector at point \mathbf{x} due to the unit discontinuity at ξ ,

$$\Phi_{ij} = \frac{(1-\nu)}{4\pi R^2} \left[\frac{(1-\nu)}{(1+\nu)} (n_i R_j - n_j R_i + n_k R_k d_{ij}) + \frac{2n_k}{R^2} R_k R_i R_j \right] \quad (4.6)$$

where ν is the Poisson's ration, n_i is the unit normal to the discontinuity and $R_i = x_i - \xi_i$ and $R^2 = R_1^2 + R_2^2$. The integration is performed over the length of the discontinuity, s . Employing the coordinate system shown in Figure 15, and assuming that on the average sense crazes are horizontal at any point within every square of the grid (Figure 15), $n_1=0$, $n_2=1$, and $R_1=(x_1-\xi_1)$, $R_2=(x_2-\xi_2)$.

To continue, the shape of the discontinuity $b(\xi)$ should be identified. With reference to the Figure 15, the crazes within a square are taken horizontal and segregated to a single discontinuity of length equal to the length of the square. The width of the discontinuity is assumed to be equal to the product of the some reference opening b_0 , and the number of crazes within the respective square. Thus, at the typical square of i_{th} column and j_{th} row with a number of crazes P_{ij} which is measured experimentally the opening of an effective discontinuity is,

$$b_{ij}^g(\xi) = b_0 P_{ij}(\xi) \quad (4.7)$$

Accordingly, the vertical displacement at a point $\mathbf{x}(x_1, x_2)$ due to the effective discontinuity within a square whose center is located at $\xi(\xi_1, \xi_2)$ is obtained by combining Equations (4.5) to (4.7),

$$U_2^{(ij)}(\mathbf{x}, \xi) = b_0 P_{ij} \int_{(\xi_1)_{j-0.5}}^{(\xi_1)_{j+0.5}} \frac{(1+\nu)}{4\pi R^2} \left[\frac{(1-\nu)}{(1+\nu)} (x_2 - \xi_2) + \frac{2(x_2 - \xi_2)^3}{R^2} \right] d\xi_1 \quad (4.8)$$

where c is the size of the square in the grid (Figure 15b). The displacement at the grips of the specimen due to a discontinuity was obtained by a numerical integration of (4.8) using a standard routine, at $x_2=h$, where h is half the specimen height.

The total displacement at the grips is obtained by summing up the contributions of the individual displacements caused by each of the effective discontinuities within the array,

$$U_2(x_1, h) = \sum_{i=1}^{N_1} \sum_{j=1}^{N_2} U_2^{(ij)}(x_1, h) \quad (4.9)$$

The average displacement at the grips due to the damage zone Δ_{craze} , is obtained by averaging the displacements across the specimen width B ,

$$\Delta_{\text{craze}} = \frac{2}{B} \int_0^B U_2(x_1, h) dx_1 \quad (4.10)$$

A parameter that remains to be identified is a reference craze opening b_0 (Equation 4.7). Due to difficulties in evaluating such a quantity in the experimental studies, an opening of $b_0 = 1 \mu\text{m}$ was assumed. It can be seen from Equation (4.7) that the results are directly proportional to b_0 . Thus, the trends of the energy release rate remain unaltered.

Values of the characteristic size l_a , cycle number, and energy release rates A , (Equation 4.1) for two loading conditions C1 and C2 are shown in Table V. Using these energy values, the evolution of the damage zone size, $\Delta l_a / \Delta N$, isotropic expansion, $\Delta e / \Delta N$, and distortion, $\Delta d / \Delta N$ [1], are shown in Figures 16 (conditions C1) and 4 (conditions C2). The data in these Figures suggest that the overall growth behavior of the damage zone before crack initiation decreases monotonically. This trend is consistent with the growth behavior of an average damage density before crack initiation (sec. 3). Moreover, it is interesting that the monotonic decrease shown in Figures 16 and 17 resembles the behavior of small cracks observed in different materials [53].

The correlations shown in Figures 16 and 17, although approximate, illustrate the trends of damage growth before crack initiation. However, criteria for crack initiation can not be easily formulated in terms of some Griffith's like criteria. That is, for the fracture process investigated in this work, an energy release rate (or stress intensity

factor) quantity associated with crack initiation would depend on the specific energy for craze formation, the amount of crazes as a function of time and applied loads, as well as the interactions between the crazes and the stress concentrator. It is difficult, however, to evaluate these contributions with the existing experimental and analytical methods. Answers to these questions should await the development of more refined analytical methods and improved experimental techniques.

The experimental results of this work [25] have shown that damage before crack initiation consisted of a core of dense crazing and a peripheral less dense zone of crazing. While the pattern of the peripheral crazes depended upon the applied load, the density within the core zone was independent of the loading conditions. In the remaining of the paper, this later observation is combined with principles based on microstructural models for defect nucleation and certain assumptions to describe damage accumulation in the core zone and the instance of crack initiation.

KINETIC CHARACTERISTICS OF DAMAGE IN THE CORE ZONE

Experimental and analytical investigations have shown that fracture of polymeric materials is due to thermal fluctuations on the molecular level. Thus, reaction rate theory has been employed to model their behavior. The exact mechanisms that lead to failure of these materials, however, are not known a priori. Consequently, various hypotheses have been proposed. In one of them, it is assumed that the primary molecular mechanism giving rise to fracture is scission of polymer molecules under stress. In such a case, an activation energy is related to the energy of thermal destruction [22, 45, 49]. Another hypothesis is based on polymer chain slippage and rearrangement upon stress [51]. For such processes an energy barrier is determined by the rate of polymer molecules slipping over each other. A combination of bond breakage and slippage has also been proposed [49, 51]. The extent to which either of these two mechanisms dominates depends primarily on material and test temperature. However, it is difficult to quantify their contributions. Thus, they are usually treated as a mechanism with a single energy barrier. Whatever the exact mechanisms may be, it appears that models based on reaction rate theory describe certain features of polymer fracture reasonably well, although, certain modifications and assumptions may be necessary to accommodate experimental observations [48].

To model the process of damage accumulation within the core zone (Figure 14), it is assumed that on the submicroscopic level fracture is the result of thermal fluctuations of polymer chain segments which form crazes. Within the crazes chain rupture and/or chain pull - out occur which reduce the load bearing capacity of the

fibrils thus, causing additional ruptures or chain pull - out. This is the stage of submicrocrack development. When the number of submicrocracks reaches a critical level, a macroscopic crack appears.

To describe this process in quantitative terms, it is assumed that there exists a certain number of elements R_0 within the area around the notch tip where submicrocracks may nucleate [47]. Therefore, the rate of submicrocrack growth $dR(t)/dt$, is postulated according to the absolute rate theory,

$$\frac{dR(t)}{dt} = K_b(R_0 - R(t)) \quad (4.11)$$

where K_b [sec^{-1}] can be looked upon as the rate of submicrocrack accumulation. It should be noted that the contribution of defect healing is not taken into account in the rate equation. It is shown later in this work that its contribution is much smaller in comparison to that due to submicrocrack nucleation. Thus, it can be safely neglected in the present analysis.

In the experimental studies, the extent of crazes in the core zone was measured at different times before crack initiation. Therefore, it is assumed that the amount of submicrocracks at any time prior to crack initiation is proportional to the extent of crazes within the core zone. Furthermore, having in mind that damage density within the core reached a constant value [25], independent of the loading conditions, a normalized damage parameter is introduced in the following form,

$$r(t) = \frac{R(t)}{R_c} \quad (4.12)$$

where R_c is the density of submicrocracks at initiation. On the basis of this definition $r(t)$ takes the following limiting values,

$$r(t=0) = 0 \quad \text{corresponds to no damage} \quad (4.13a)$$

$$r(t=\tau_i) = 1 \quad \text{corresponds to crack formation} \quad (4.13b)$$

where τ_i is the crack initiation time. Accordingly, Equation (11) may be written as,

$$\frac{dr(t)}{dt} = -K_b r(t) + K_b r_0 \quad (4.14)$$

where the $r_0 = R_0/R_c$ is a constant.

Assuming that the submicroscopic mechanisms taking place during damage accumulation are driven by thermal fluctuations and the applied stress, the rate constants for nucleation and healing are given by [43],

$$K_b = \frac{1}{\tau_0} \exp[-(U_0 - \Delta U/2)/kT] \quad (4.15a)$$

$$K_h = \frac{1}{\tau_0} \exp[-(U_0 + \Delta U/2)/kT] \quad (4.15b)$$

Here $1/\tau_0$ is the vibration frequency, which for most solids it is found to be in the order of 10^{13}sec^{-1} ; U_0 [J/mole] is the activation energy due to thermal fluctuations; ΔU [J/mole] is the change in activation energy due to the applied stress; $k=1.38 \times 10^{-21}$ [J/K] is the Boltzmann's constant; T [K] is the temperature. The terms $\exp[-(U_0 - \Delta U/2)/kT]$ and $\exp[-(U_0 + \Delta U/2)/kT]$ represent the probabilities that a weak region is at an energy level $U_0 - \Delta U$ or $U_0 + \Delta U$.

To estimate the rate constant from the above expressions both energy quantities U_0 and ΔU should be evaluated. One way to achieve this goal is to use the methods of statistical physics that would require knowing enough about the types of microdefects, their distribution in space and time, and the range of their interaction. Such an effort, however, is very difficult to achieve for practical systems. To circumvent this problem, the dependence of the energy barrier on stress is usually approximated with potentials appropriate to a particular molecular mechanism of failure [54]. In this work we resort to an empirical method for evaluating U_0 and ΔU that has been shown to apply well in different materials.

Extensive experimental research on various solids subjected to static or cyclic tensile stress σ , have demonstrated that the time to fracture τ_i , can be described by [22, 55],

$$\tau_i = \tau_0 \exp\left(\frac{U_0 - \gamma\sigma}{kT}\right) \quad (4.16)$$

where γ [J/mole·MPa] is a parameter that describes the degree of non uniformity of stress distribution in the loaded specimen. The magnitude of U_0 has been found to coincide with the interatomic binding energy of various materials [22]. Both quantities U_0 and γ are obtained by fitting Equation (4.16) to experimental results of time to fracture where σ is taken as the applied stress in creep experiments and as the stress amplitude in the case of fatigue tests. Evidently, the time to fracture given by Equation

(4.16) is equal to the inverse of the rate constant in Equation (4.15a) when the reduction in the activation energy is linearly related to the stress, i. e., $\Delta U = 2\gamma\sigma$.

Although, Equation (4.16) describes failure times of smooth specimens under constant and fatigue loads very well, it has not been applied to crack initiation times from a stress concentrator. This may be because in smooth specimens the applied stress field is assumed uniform and thus, satisfies the requirements of the equilibrium Boltzmann's statistics. On the other hand, the high stress gradients around a stress concentrator, presumably violate the requirements of Boltzmann's statistics. Accordingly, it may be physically unrealistic at first to apply (4.16) to data of crack initiation times from a stress concentrator. The experimental results have shown a relatively large number of crazes at the core zone (Figure 14), and that this density reaches a load independent level at the instance of crack initiation (sec. 3). Thus, it is assumed that the stress level over the core zone (Figure 14) immediately ahead of the notch tip is uniform and proportional to the amplitude to the applied stress. In terms of fracture mechanics, this is similar to considering the layer of damage as a cohesive zone similar to that in the Dugdale - Barenblatt model [56].

To examine the crack initiation times according to (4.16) the stress parameter is approximated by the level of mean stress, $\sigma_a = (\sigma_{\max} - \sigma_{\min})$. Under the assumptions stated in the preceding paragraphs, parameters U_0 and γ are evaluated by fitting the experimental data on crack initiation reported in [25]. For this purpose, Equation (4.16) is written as,

$$\sigma_a = -\frac{kT}{\gamma} \ln \tau_i + \frac{kT}{\gamma} \ln \tau_0 + \frac{U_0}{\gamma} \quad (4.17)$$

Using the data in Figure 13 [1], a plot of σ_a against $\ln \tau_i$ for five experiments resulted in, $\frac{kT}{\gamma} = 1.46$ and $\frac{kT}{\gamma} \ln \tau_0 + \frac{U_0}{\gamma} = 25.20$. Solving for γ and U_0 one obtains $\gamma = 2.08$ kJ/MPa·mole and $U_0 = 117.13$ kJ/mole.

It has been reported that for PS, the energy for thermal destruction is about 230 kJ/mole [22] and an activation enthalpy for secondary chain motions below glass transition temperature about 65 kJ/mole [34]. If the activation energy indicates the types of submicroscopic mechanisms, a value of $U_0 = 115.6$ kJ/mole suggests that secondary chain motions as well as chain scission are possible rate determining processes which lead to crack initiation. This is consistent with the observation that dense crazing precedes crack initiation.

The preceding analysis of the experimental data on crack initiation times has resulted in the evaluation of an activation energy U_0 and the changes due to the applied stress $\Delta U = 2\gamma\sigma_a$. Therefore, the rate constants K_b and K_h can be calculated. Using Equations (15) and the values of U_0 and γ obtained from the foregoing analysis it is obtained, $K_b/K_h \sim 10^4$. That is, healing processes may be neglected in the rate of submicrocrack development. Accordingly, since K_b is independent of time, the solution of Equation (4.14) is,

$$r(t) = r_0 + C \exp(-K_b t) \quad (4.18)$$

Imposing the condition, $r(0) = 0$, one obtains,

$$r(t) = r_0 [1 - \exp(-K_b t)] \quad (4.19)$$

The value of r_0 is estimated from the condition $r(t=\tau_i) = 1$. For conditions C1 and C2, it was found that $r_0 \approx 1.58$, while for C2, $r_0 \approx 2.00$. This larger value was attributed to the fact that the crack initiation time under conditions C2 was about 40% smaller than that predicted by (4.16). The solid lines in Figure 18 represent Equation (4.19) and the points are the experimental data of the normalized density for loading conditions C1(a), C2(b) and C3(c), respectively. Because of the large differences in the crack initiation times, the data for each condition are plotted separately for the sake of visual clarity. The data in Figure 18 demonstrate that Equation (4.19) fits the data reasonably well. Expressions similar to (4.19) have been also reported in [44, 45, 47] for creep loads of smooth specimens.

TABLE V: Cycle number, Characteristic Size and Energy Release Rates, A , due to Damage Growth for two Loading Conditions.

Configuration	Cycle Number	Characteristic Size, μm	Energy Release Rate, J/m^2
Conditions C1:			
1	27,000	42	
2	50,000	52	17.5
3	150,000	80	38.0
4	300,000	120	73.0
Conditions C2:			
1	10,050	58	
2	19,000	87	32.0
3	30,000	117	105.0

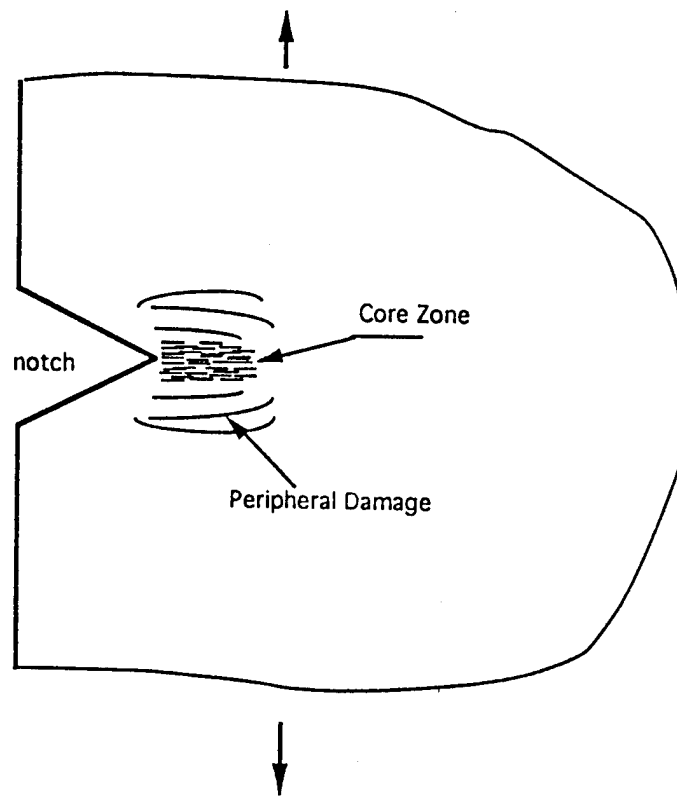
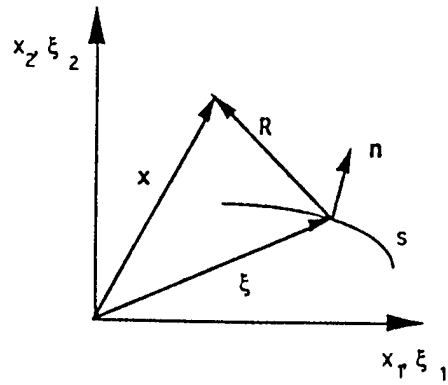
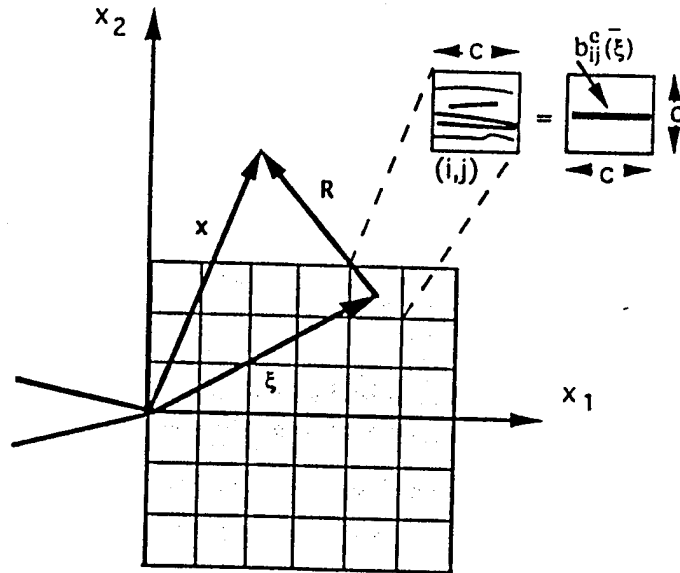


Fig. 14 Schematic of a damage zone around a V- notch



(a)



(b)

Fig. 15

(a) Illustration of a displacement response at point x , due to a discontinuity at ξ given by expression (5), (b) Schematic showing the approximation of discontinuities within a rectangle (see text for details)

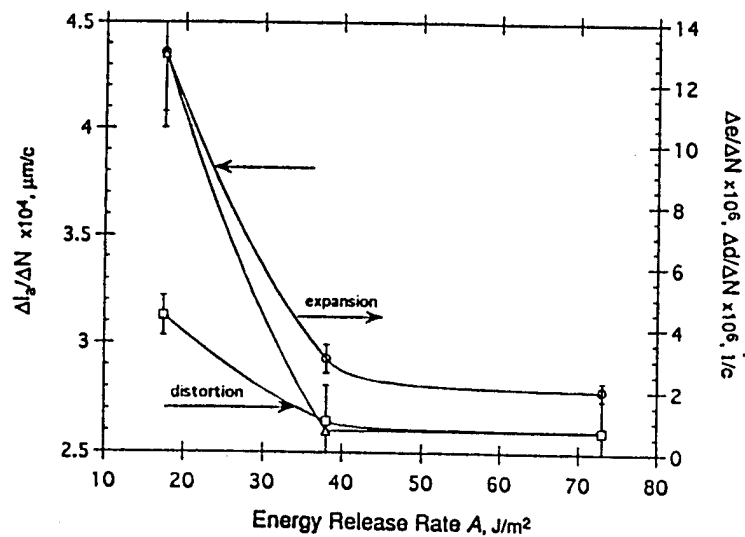


Fig. 16 Growth rates of the characteristic size, isotropic expansion and distortion of the damage zone vs. energy release rate (Conditions C1)

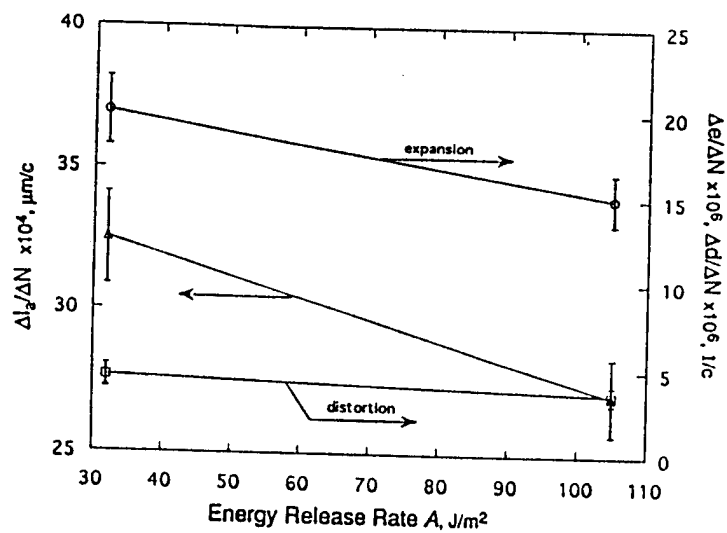


Fig. 17 Growth rates of the characteristic size, isotropic expansion and distortion of the damage zone vs. energy release rate (Conditions C2).

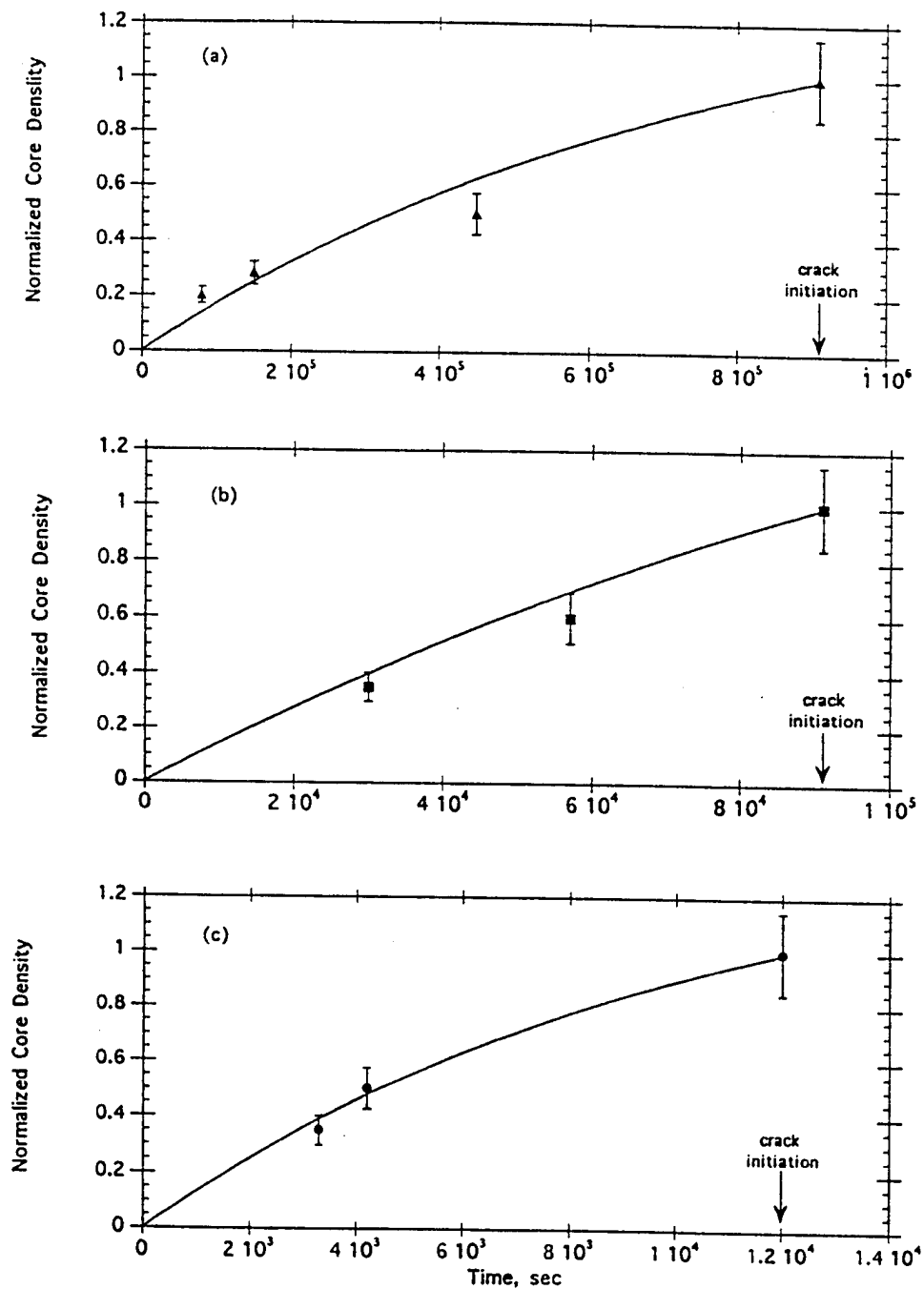


Fig. 18 Evolution of normalized damage density in the core vs. time for three loading conditions, a (C1), b (C2), and c (C3).

REFERENCES

1. J. M. Barsom and S. T. Rolfe, in *Fracture and Fatigue Control in Structures*, 2nd Edition, Prentice Hall, Englewood Cliffs, N. J., (1987).
2. R. W. Hertzberg and J. A. Manson, in *Fatigue in Engineering Plastics*, Academic Press, New York, N. Y. (1980).
3. R. O. Ritchie, *International Metals Reviews*, 5 (1979) 205.
4. C. J. Beevers and R. L. Carlson, in *Fatigue Crack Growth 30 years of Progress*, R. A. Smith ed., Pergamon Press, N.Y. (1986) 89.
5. D. L. Davidson and S. Suresh, eds., in *Fatigue Crack Growth Threshold Concepts*, The Metallurgical Society of AIME, Philadelphia, PA (1984).
6. R. O. Ritchie, in *Advances in Fracture Research, Proc. ICF4*, S. R. Valluri et. al. eds., Pergamon Press, N.Y., 1 (1984) 235.
7. T. C. Lindley and K. J. Nix, in *Fatigue Crack Growth 30 years of Progress*, R. A. Smith ed., Pergamon Press, N.Y. (1986) 53.
8. W. A. Wood, in *Treatise on Materials Science and Technology* Vol. 5, H. Herman, ed., Academic Press, N. Y. (1974) 129.
9. O. Helgeland, *Journal of Institute for Metals* 93 (1965) 570.
10. M. E. Mackay, T. G. Teng and J. M. Schultz, *Journal of Materials Science*, 14 (1979) 221.
11. N. J. Mills and N. Walker, *Journal of Materials Science*, 15 (1980) 1832.
12. M. Kitagawa, *Journal of Materials Science*, 17 (1982) 2514.
13. J. Botsis, A. Chudnovsky and A. Moet, *International Journal of Fracture*, 33 (1987) 263.
14. M. Kachanov, E. L. E. Montagut, and J. P. Laures, *Mechanics of Materials*, 10 (1990) 59.
15. G. I. Barenblatt and L. R. Botvina, *Soviet Materials Science* (English translation of Fiziko-Khimicheskaya Mehanika Materialov 22 (1986) 52.
16. A. Chudnovsky, *10th U. S. National Conference on Applied Mechanics*, Ed. J. P. Lamb, ASME, Austin, Texas, 1986, p. 97.
17. J. Botsis and X. Q. Zhang, *Journal of Materials Science*, 26 (1991) 1253.
18. J. Botsis, *Journal of Materials Science*, 24 (1989) 2018.
19. G. Margaritis and J. Botsis, *Engineering Fracture Mechanics*, 40 (1991) 1123.
20. V. S. Kuksenko and V. P. Tamuzs, in *Fracture Micromechanics of Polymer Materials*, Martinus Nijhoff, The Hague, (1981).

21. F. Bueche, *Journal of Applied Physics*, 29 (1958) 1231.
22. S. N. Zhurkov, *International Journal of Fracture*, 26 (1984) 295.
23. C. N. Robinson, P. H. Graham, and F. C. Moore, in *Application of Reaction Rate Theory to Solid Propellant Mechanical Behavior*, Vol. 2, Atlantic Res. Corp., Technical Report AFRPL-TR-69-124, (1969).
24. V. R. Regel, and A. M. Leksovsky, *International Journal of Fracture Mechanics*, 3 (1967) 99.
25. J. Botsis and C. Huang, *International Journal of Fracture*, Submitted, (1993).
26. J. W. Hutchinson, *Acta Metallurgica*, 35 (1987) 1605.
27. M. Ortiz, *Journal of Applied Mechanics*, 54 (1987) 54.
28. C. H. Wu, *Journal of Applied Mechanics*, 55 (1988) 736.
29. A. Chudnovsky, and M. Kachanov, *Applied Engineering Science Letter*, 21 (1983) 1009.
30. A. Chudnovsky, A. Dolgopolsky, and M. Kachanov, *International Journal of Solids and Structures*, 23 (1987) 1.
31. H. Horii, and S. Nemat-Nasser, in *Advances in Aerospace Structure, Materials and Dynamics*, Edited by U. Yuceoglu, et. al., ASME (1983) 111.
32. M. Kachanov, *International Journal of Fracture*, 28 (1985) R11.
33. A. A. Rubinstein, *Journal of Applied Mechanics*, 53 (1986) 505.
34. A. Chudnovsky and Shaofu Wu, *International Journal of Solids and Structures*, 29 (1992) 1699.
35. A. Chudnovsky and M. Ben Ouezdon, *International Journal of Fracture*, 37 (1988) 3.
36. M. R. Lin, M. E. Fine, and T. Mura, *Acta Metallurgica*, 34 (1986) 619.
37. L. M. Kachanov, *Introduction to Continuum Damage Mechanics*, Martinus Nijhoff Publishers, (1986).
38. A. Benallal, R. Billardon and J. Lemaitre, in '*Advances in Fracture Research, Proc. ICFG*', S. R. Valluri et.al. eds., Pergamon Press, N.Y., 1984, Vol. 4, p. 3661.
39. A. Chudnovsky, in '*Workshop on a Continuum Mechanics Approach to Damage and Life Prediction*', D. C. Stouffer et.al. eds., Carrollton, Kentucky (1980).
40. P. W. Whaley, '*Entropy Production During Fatigue as a Criterion for Failure*', ONR Technical Report No. 1, 1983.
41. D. R. Curran, L. Seaman and D. A. Shockey, *Physics Reports*, 147 (1987) 253.

42. P. Meakin, 'Simple Kinetic Models for Materials Failure and Deformation', in *Statistical Models for the Fracture of Disordered Media*, Eds. H. J. Herrmann and S. Roux, Elsevier Science Publishers, North Holland, (1990) 291.
43. A. S. Krausz and H. Eyring, *Deformation Kinetics*, John Wiley and Sons, New York, N. Y. (1975).
44. A. C. Hansen and J. Baker-Jarvis, *International Journal of Fracture*, 44 (1990) 221.
45. S. N. Zhurkov and V. E. Korsukov, *Journal of Polymer Science, Polymer Physics*, 12 (1974) 385.
46. S. N. Zhurkov, *International Journal of Fracture*, 1 (1965) 311.
47. V. A. Petrov, *Soviet Physics, Solid State*, 7 (1984) 26.
48. K. L. DeVries, B. A. Lloyd and M. L. Williams, *Journal of Applied Physics*, 42 (1971) 4644.
49. F. Bueche, *Journal of Applied Physics*, 28 (1957) 784
50. F. Bueche, *Journal of Applied Physics*, 26 (1955) 1133
51. I. Becht, K.L. DeVries and H. H. Kausch, *European Polymer Journal* , 7 (1971) 105.
52. H. Tada, P. C. Paris, and G. P. Irwin, *Stress Analysis of Cracks Handbook*, Del Research Corp., Helertown PA, (1975)
53. R. O. Ritchie and J. Lankford, *Small Fatigue Cracks*, The Metallurgical Society of AIME, Philadelphia, PA (1986).
54. S. L. Phoenix and L-J. Tierney, *Engineering Fracture Mechanics*, 18 (1983) 192.
55. V. R. Regel, and A. M. Leksovsky, *International Journal of Fracture Mechanics*, 3 (1967) 99.
56. K. Hellan, *Introduction to Fracture Mechanics*, McGraw-Hill, New York, N. Y. (1984).
57. N. G. McCrum, B. E. Read and G. Williams, *Anelastic and Dielectric Effects in Polymeric Solids*, John Wiley and Sons, London (1967).